frontiers | Frontiers in Earth Science

ORIGINAL RESEARCH
published: 14 July 2022
doi: 10.3389/feart.2022.929599

Spatiotemporal Variation of Late Quaternary River Incision Along the Heihe River in the Northeastern Tibetan Plateau, Constrained by Dating Fluvial Terraces

Xilin Cao[1,2], *Xiaofei Hu*[2]*, *Baotian Pan*[2] *and Zhijun Zhao*[1]

[1]*Jiangsu Center for Collaborative Innovation in Geographical Information Resource Development and Application, School of Geography, Nanjing Normal University, Nanjing, China,* [2]*Key Laboratory of Western China's Environmental Systems (Ministry of Education), College of Earth and Environmental Sciences, Lanzhou University, Lanzhou, China*

Rates of river incision are widely used to track changes in rock uplift rate and climate over time and space. However, the relationship between the spatiotemporal variation of river incision and past tectonic or climatic processes is still unclear. Here, we focus on the spatial patterns of river incision in the interior and front of the Qilian Shan in the northeastern Tibetan Plateau. A sequence of late Quaternary terraces is well preserved along the Heihe River across the central Qilian Shan. We complement existing chronologic data with five new optically stimulated luminescence ages and one cosmogenic radionuclide ^{10}Be exposure age of terrace abandonment. At the mountain front, the river incision rate was ~1 mm/yr over the past 100 kyr, while the range was from 2 to 7 mm/yr during the Holocene. We attribute the fast incision rates during the Holocene to the progressive decrease of the river gradient induced by the warm and wet Holocene climate. In the interior of the mountains (the Qilian basin site), the river incision rates were close to 1 mm/yr since ~53 ka, suggesting that the upstream incision rate remained stable from the late Pleistocene to the Holocene. This observation further suggests that the adjustment of the climate-induced longitudinal river profile is limited to the downstream reach, especially along the front of the mountain range. We conclude that the long-term incision rate (during the late Pleistocene) is explained by ongoing uplift driven by fault activity, which determines the background rate of fluvial incision (~1 mm/yr). On the other hand, denudation rates on the millennial timescale estimated by previous studies in this region are < 1 mm/yr, suggesting that landscape-scale erosion lags behind trunk river incision.

Keywords: fluvial terrace, river incision, Heihe River, Qilian Shan, northeastern Tibet

OPEN ACCESS

Edited by:
Hao Long,
Nanjing Institute of Geography and Limnology (CAS), China

Reviewed by:
Honghua Lu,
East China Normal University, China
Yiquan Li,
Nanjing University, China

***Correspondence:**
Xiaofei Hu
feixhu@lzu.edu.cn

Specialty section:
This article was submitted to Quaternary Science, Geomorphology and Paleoenvironment, a section of the journal Frontiers in Earth Science

Received: *27 April 2022*
Accepted: *22 June 2022*
Published: *14 July 2022*

Citation:
Cao X, Hu X, Pan B and Zhao Z (2022) Spatiotemporal Variation of Late Quaternary River Incision Along the Heihe River in the Northeastern Tibetan Plateau, Constrained by Dating Fluvial Terraces. Front. Earth Sci. 10:929599. doi: 10.3389/feart.2022.929599

1 INTRODUCTION

Average river incision rates are closely related to specific spatial and temporal scales (Daniels, 2008; Finnegan et al., 2014). On the timescale of millions of years (Myr), river incision is sensitive to the rock uplift rate, modified by tectonic or isostatic processes (Pan et al., 2003; Kirby and Whipple, 2012). On the timescale of several thousand years (kyr), river incision can vary with the ratio of sediment flux to water flux, as well with the vegetation cover, modified by glacial or interglacial cycles

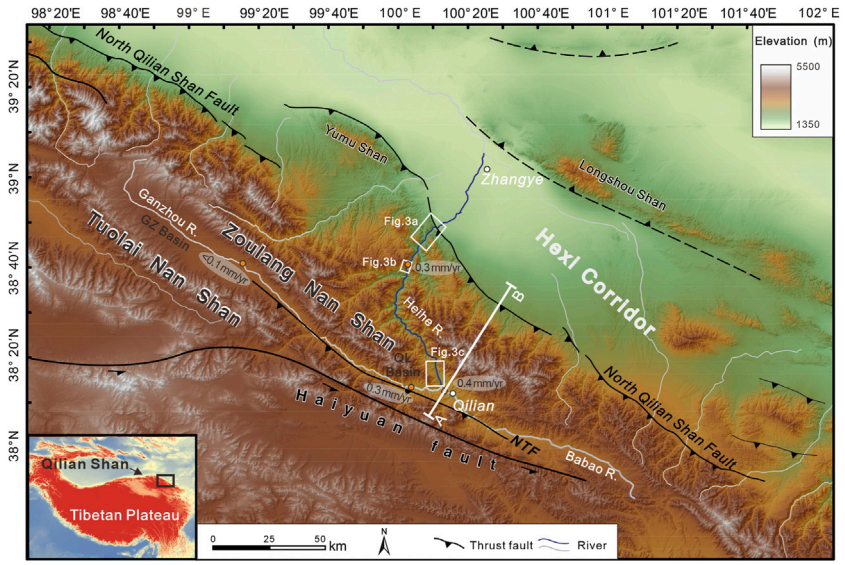

FIGURE 1 | Topographic map of the northeastern Tibetan Plateau (derived from 90 m SRTM data). The blue line indicates the fluvial reach shown in **Figure 2B**. The orange dots represent partial erosion rates estimated from cosmogenic ^{10}Be concentrations in river sediments (Palumbo et al., 2011; Hetzel, 2013; Hu et al., 2015a). NTF, North Tuolai Shan Fault; GZ Basin, Ganzhou River Basin; QL Basin, Qilian Basin.

(Ferrier et al., 2013). Moreover, a major river always flows through different tectonic zones, which complicates the relationship between river incision and tectonic or climatic processes (Craddock et al., 2010).

Over the past few decades, several studies have documented recent rapid incision rate events in northeastern Tibet that are probably linked to global climate change. For example, along the mountain front of the Qilian Shan and the Tien Shan, the deeply entrenched piedmont and the fast river incision are largely related to the warm and wet climate of the Holocene, rather than to tectonic forcing, which was shown to account for only 10% of the total incision (Poisson and Avouac, 2004; Hetzel et al., 2006; Lu et al., 2020). These authors further attributed the fast river incision to the progressive reduction of the river gradient along the mountain front. However, it is unclear whether the incision process continues to expand upstream, or if it restricted to the downstream reach. Quantifying changes in river incision rate over time and space is the primary method used for reconstructing this process.

In this study, we combined field observations, digital topographic analysis, and optically stimulated luminescence and cosmogenic radionuclide dating of multiple levels of fluvial terraces preserved along the Heihe River to quantify the spatial and temporal variation of river incision in northeastern Tibet during the Quaternary (**Figure 1**). We focus on the terraces located in the interior and the front of the Qilian Shan. These terraces provide average incision rates of the trunk valley of the Heihe River on timescales of 100–10 kyr. Furthermore, the distribution of the fluvial terraces and the spatial variation of their height above the river provide important information on the spatiotemporal pattern of river incision, which may help differentiate between tectonic and climatic forcing of river incision (Burbank et al., 1996).

2 STUDY AREA

Along the northeastern margin of the Tibetan Plateau, the Qilian Mountains are composed of several parallel NW-SE-trending ranges (e.g., the Zoulang Nan Shan and Tuolai Nan Shan, **Figures 1**, **2**), separated by thrust-fold systems. From the Hexi Corridor to the Qaidam Basin, the mountain ranges have a width of ~300 km. Multiple lines of evidence indicate that the uplift of the Qilian Mountains was caused by the extrusion of the Tibetan Plateau from the Early Miocene (Bovet et al., 2009; Zheng et al., 2010). The North Qilian Shan Fault (NQF, **Figure 1**) separates the mountain range and the foreland basin (Hexi Corridor) and dominates the uplift of the Qilian Mountains. The vertical slip rate of this boundary fault is estimated as 0.7–1.5 mm/yr, based on studies of late Quaternary geomorphic surfaces (e.g., Yang et al., 2018; Cao et al., 2021).

Our study area is in the northernmost range of the Qilian Shan and Zoulang Nan Shan, between the longitudes of 99°30′E and 100°20′E (**Figure 1**). The Heihe River drains the Zoulang Nan Shan and enters the Hexi Corridor (**Figure 2**). The segment up to the NQF is treated as the upstream reach, located in the mountain area with an average elevation of ~4,000 m. The upstream reach has two large tributaries: the Ganzhou River and the Babao River (**Figure 1**). The Ganzhou River drains eastward, joining the smaller and westward-flowing Babao River near the city of Qilian. The combined river then turns northward, and cross-cuts the NW-SE-oriented range of the Zoulang Nan Shan, producing a transverse drainage pattern. Specifically, the upper Ganzhou River valley is located at a piggy-back basin filled with Late Mesozoic and Quaternary deposits, with the thickness of the Quaternary deposits exceeding 400 m (Li, 1994). Cosmogenic nuclide data from the southern Zoulang Nan Shan show that

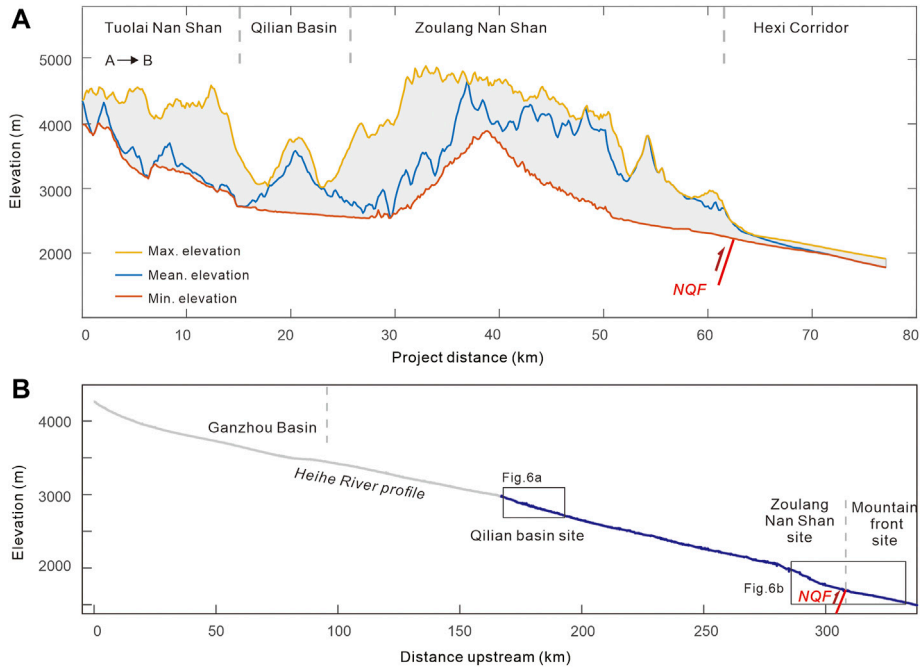

FIGURE 2 | (A) Swath profile (10 km × 10 km) across the Tuolai Nan Shan-Hexi Corridor. **(B)** Longitudinal profile of the Heihe River. Terraces along the blue reach are divided into three segments: Qilian basin site, Zoulang Nan Shan site, and mountain front site. Locations of the swath profile and the blue reach are shown in **Figure 1**. NQF, North Qilian Shan Fault.

millennial-scale erosion rates are as low as ~0.02 mm/yr, owing to the deposition of Quaternary sediments in the Ganzhou basin (upper Heihe River valley, Hetzel, 2013).

3 METHODS

3.1 Correlating and Classifying the Terraces

The terraces of the Heihe River have been extensively studied (Li et al., 1995; Li et al., 1999; Ren et al., 2019; Hu et al., 2021). Here, we use the labels Y-T1 to Y-T6 for the major terraces at the Zoulang Nan Shan–Mountain front sites (**Figure 2B**), and Q-T1 to Q-T6 for the major terraces of the Qilian basin site. We first mapped the terrace distribution on three segments along the Heihe River (the mountain front site, the Zoulang Nan Shan site, and the Qilian basin site; **Figures 2B**, **3**) using satellite imagery from Google Earth and detailed field surveys. Field investigations validated the terrace level, height, location, and extent of each mapped terrace, in addition to verifying the relative terrace ages based on geometric and topographic relationships. Correlation of terraces was primarily based on the continuity of the surface, the relative height of the terrace above the riverbed, and the terrace ages. The terraces were numbered in ascending order, from low to high: e.g., Y-T1 to Y-T6 at the mountain front and Zoulang Nan Shan sites. Note that the Qilian reach is one of the sites documented in our previous study (Hu et al., 2021), which used the labels T1 to T6 for the major terraces at the Qilian basin site. In the present study, we have modified the previous nomenclature because we identified new lower terraces. Adjacent to the river, three lower terraces were named Q-T1a, Q-T1b and Q-T1c. Through detailed field investigations (**Figure 3B**), the terrace numbers Q-T1b, Q-T2 to Q-T6 in this study respectively correspond to terraces T1 to T6 in Hu et al. (2021).

The elevations of the terrace surfaces (mainly the top of the fluvial gravels), strath surfaces, and the modern riverbed were surveyed using differential GPS (Trimble 5800), with uncertainties of less than 10 cm in the vertical direction. The higher terrace levels in the Qilian basin site were investigated in our previous study (Hu et al., 2021), and thus we adopted the survey data in the present study. For the Zoulang Nan Shan site, the terraces are discontinuous and thus several transects were established (**Figure 4**). Y-T4 and Y-T3, specifically, are widely spaced and extend for several kilometers in the foreland basin. Therefore, the terrace elevations were determined by both GPS surveying and DEM extraction (12.5-m ALOS PALSAR data, https://search.asf.alaska.edu/#/).

3.2 Dating the Terraces

The river incision rate is the ratio between the height of the terrace tread above the modern river level and the age of terrace formation (Burbank and Anderson, 2011). We determined the abandonment ages of the fluvial terraces based on previous work, as well as with our new data. The new terrace ages were determined using optically stimulated luminescence (OSL) and *in-situ* terrestrial cosmogenic nuclide (TCN) dating methods.

Floodplain sediments are deposited above the fluvial gravels on each terrace, and thus the dating was conducted on these floodplain sediments. Five new OSL samples were collected in this study.

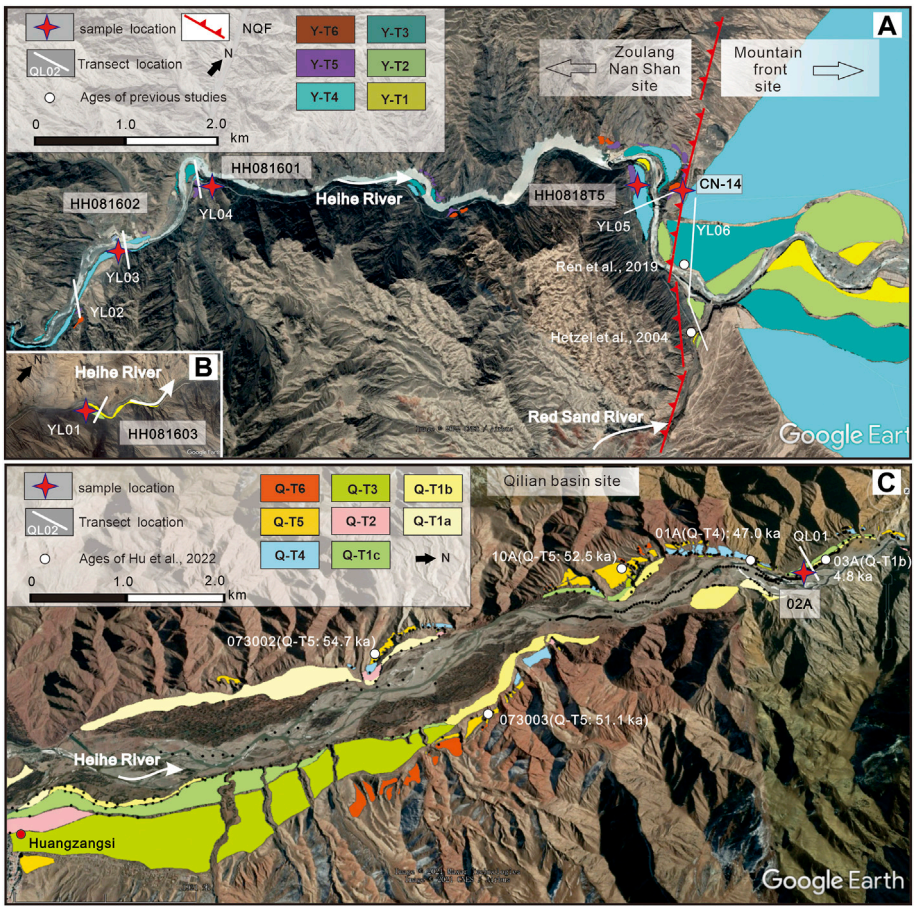

FIGURE 3 | Terrace distributions at the Zoulang Nan Shan site, mountain front site **(A)** and Qilian basin site **(B)**, with samples and transect positions. The background is from Google Earth (Map data: Image © 2019 CNES/Airbus) and the location is shown in **Figure 1**.

Stainless steel tubes were hammered into the freshly-cleaned sections, and after extraction the tubes were sealed with aluminum foil and plastic tape. OSL sample preparation and measurements were conducted in the laboratory of the Qinghai Institute of Salt Lakes, Chinese Academy of Sciences (Xining). Quartz grains (~38–63 μm) were extracted and cleaned following the procedures of Lai and Wintle (2006) and Lai et al. (2007). De was determined using the combination of the SAR protocol (Murray and Wintle, 2000) and the standardized growth curve (SGC) (Roberts and Duller, 2004). For each sample, six aliquots were measured by the SAR protocol to construct an SGC growth curve, and 11–12 additional aliquots were then measured for natural luminescence (Ln) and luminescence induced by the test dose (Tn). Sensitivity-corrected natural OSL (Ln/Tn) was projected on the SGC to yield a De. The characteristics of the De distributions for the samples are presented in **Figure 5**, and the average De was used for age calculation (**Table 1**). The decay curves, growth curves of individual aliquots, and the SGC for a representative sample (1A) are shown in **Figure 5**. The OSL signals decayed significantly during the first 1 s of stimulation (**Figure 5D**), suggesting that the OSL signal is dominated by fast components. Information on the dated samples and the age results are presented in **Table 1**.

For the highest terrace (Y-T6) along the river mouth, we collected one sample from fluvial gravels for surface exposure dating (CN-14, **Figure 3A**). Pits were excavated down to the gravel surface below the loess deposit (~45 cm). Quartz-rich clasts with diameters of 1–3 cm were selected from the gravel surface with the thickness of ~5 cm. To correct for differences in the inherited cosmogenic nuclide component, more than 30 quartz-rich pebbles were collected (Anderson et al., 1996; Niedermann and Niedermann, 2002). The quartz samples were physically and chemically purified in the Mineral Separation Laboratory of Purdue University. After target preparation, the ^{10}Be concentration was measured by accelerator mass spectrometry (AMS) at the Purdue Rare Isotope Measurement Laboratory. The two major sources of uncertainty of the cosmogenic age are the loess cover and the inheritance. Based on the ^{10}Be concentration in the Heihe trunk, we used the inheritance of $(1.15 \pm 0.06) \times 10^5$ atoms g^{-1} (Palumbo et al., 2011) for age correction, following the approach of Anderson et al. (1996). To account for the loess shielding effect, we followed the approach of Hetzel et al. (2004), with the assumption that the loess accumulated since 12 ± 2 ka and was removed only recently. ^{10}Be sample information and dating results are presented in **Table 2**.

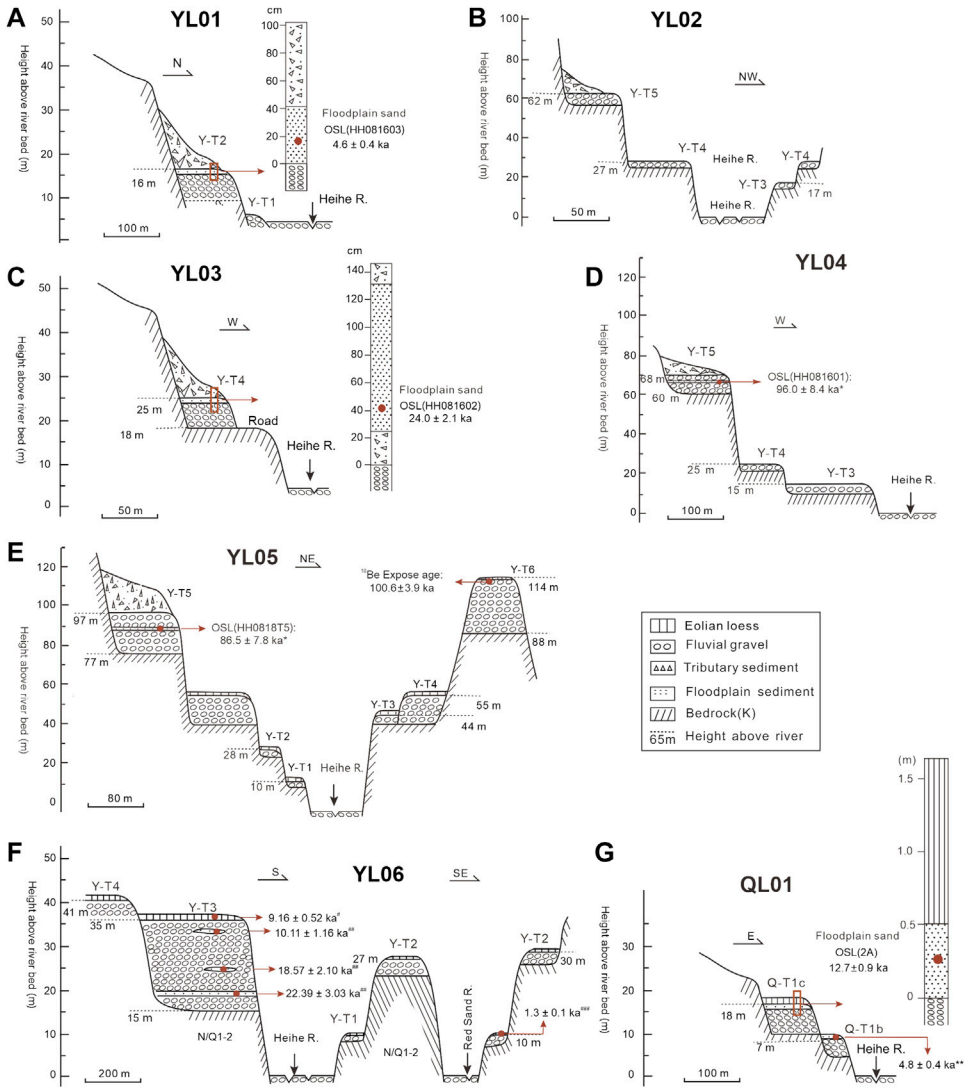

FIGURE 4 | Geomorphic transects along the Heihe River, showing the terrace staircases, the composition of each terrace level, and the locations of the samples used for terrace dating. YL01-YL05 are located in the Zoulang Nan Shan site, YL06 is located in the mountain front site and QL01 is located in the Qilian basin site. The locations of the transects are shown in **Figure 3**. Note: * indicates the excluded ages of terrace deposits; ** indicates ages from Hu et al. (2021); # indicates ages from Li et al. (1999); ## indicates ages from Ren et al. (2019) and ### indicates ages from Hetzel et al. (2004).

4 RESULTS

4.1 Fluvial Terraces Along the Heihe River

Several terraces are well preserved along the valley where the river flows through the Qilian basin, the Zoulang Nan Shan and the mountain front. By combining the previous work and the new fluvial geomorphological data of this work, we will describe the sequences of fluvial terraces along the different parts of the Heihe River.

4.1.1 Mountain Front Site

The mountain front site extends from the NQF to Zhangye city (**Figure 1**), and there are four levels of terraces along this reach (**Figure 3A**). Along transect YL06 (**Figure 4F**), GPS measurements in the field suggest that the four terraces (Y-T1 to Y-T4) are 10, 27, 35, and 41 m above the modern riverbed, respectively. For all terraces, the fluvial gravels consist mainly of rounded cobbles of sandstone, conglomerate, granite, diorite, and several metamorphic rocks. Most terrace treads are capped by 1-m-thick aeolian loess and the onset of loess deposition was in the early Holocene (Hetzel et al., 2004). Terrace profiles extracted from the DEM were consistent with the GPS measurements (**Figure 6B**). Profiles Y-T3 and Y-T4 indicate the progressive reduction of the river gradient and a decrease of the terrace spacing (**Figure 6B**). River incision decreases downstream from a maximum where the river exits the NQF to zero in the foreland.

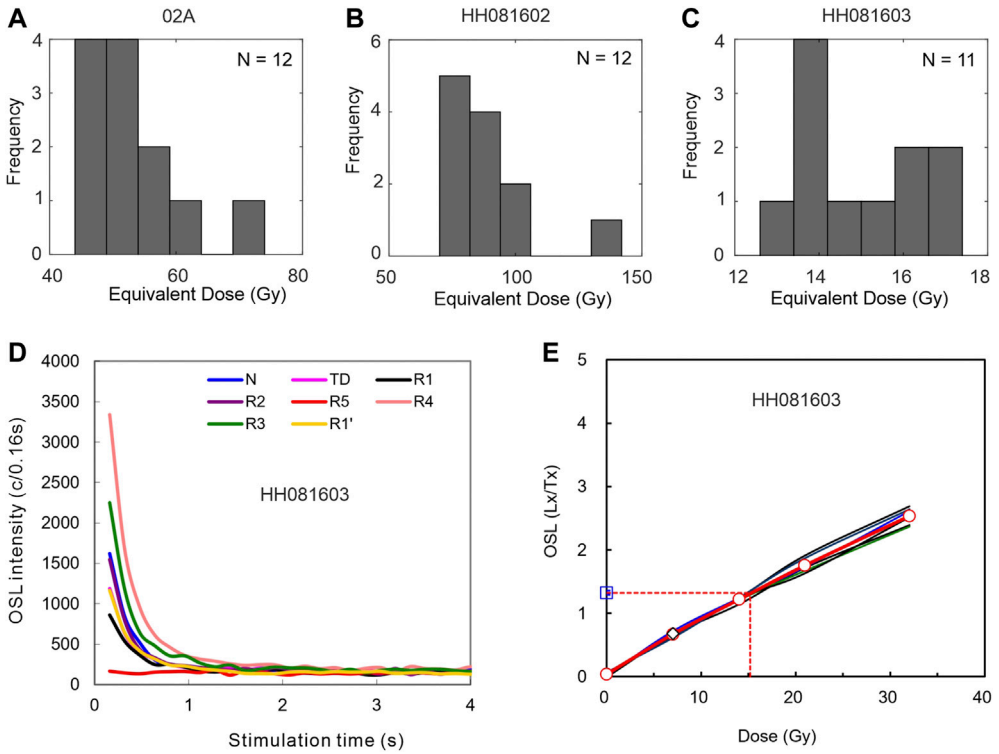

FIGURE 5 | (A–C) Equivalent dose (De) distributions. **(D)** Decay curves for sample HH081603. **(E)** OSL growth curves of individual aliquots, as well as the SGC (the bold red line), for sample HH081603.

TABLE 1 | OSL dating results.

Sample no.	Terrace	Longitude (°E)	Latitude (°N)	Altitude (m)	Equivalent dose (Gy)	Dose rate (mGy/a)	Age (ka)	Material	Location
2A	Q-T1c	100.16	38.30	2519	52.63 ± 1.52	4.15 ± 0.28	12.7 ± 0.9	Sand	Qilian basin
HH081603	Y-T2	100.03	38.66	2013	3.38 ± 0.26	15.5 ± 0.6	4.6 ± 0.4	Sand	Zoulang Nan Shan
HH081602	Y-T4	100.11	38.77	1714	3.68 ± 0.28	88.3 ± 3.7	24.0 ± 2.1	Sand	Zoulang Nan Shan
HH081601	Y-T5	100.11	38.78	1749	3.03 ± 0.23	290.7 ± 11.8	96.0 ± 8.4[a]	Sand	Zoulang Nan Shan
HH0818T5	Y-T5	100.16	38.81	1710	3.51 ± 0.27	303.4 ± 13.9	86.5 ± 7.8[a]	Sand	Zoulang Nan Shan

[a]*Indicates the excluded ages of terrace deposits. The dose rate of HH081601 and HH0818T5 are excessive that beyond the effective range of quartz dating.*

Ren et al. (2019) obtained three OSL samples from the sand lens of terrace Y-T3 (named T2 in the text). One sample from close to the top of the gravels yielded an age of ~10 ka and one sample form near the base of the gravels yielded an age of ~23 ka. The former may represent the abandonment age of terrace Y-T3 and the latter provides an age for the beginning of the Y-T3 deposit. Moreover, the age of the eolian loess atop surface Y-T3 was dated to 9.1 ka (Li et al., 1995), and thus terrace Y-T3 was formed between 9 and 10 ka. The top of the fluvial gravels of Y-T2 is 28 m above the modern riverbed and the abandonment age was suggested to be ~5 ka (Li et al., 1999). The top of the fluvial gravels of Y-T1 is 10 m above the modern riverbed, which can be correlated to the youngest terrace along the mouth of the Red Sand River, a tributary close to the Heihe river mouth (**Figure 3A**). Terrace Y-T1 of the Red Sand River has only a thin (45 cm) loess cover and the basal loess on this terrace has the age of only 1.3 ka (Hetzel et al., 2004). This indicates that the youngest terrace in this region was formed in the latest Holocene.

4.1.2 Zoulan Nan Shan Site

The Zoulan Nan Shan site is from the NQF and extends ~25 km upstream (**Figures 3A**, **6B**). Five transects were surveyed and five samples were dated. Along transect YL01 (**Figure 4A**), T2 stands 16 m above the modern riverbed with a thin layer of floodplain

TABLE 2 | ^{10}Be exposure dating results.

Sample	Sample location	Latitude (°N)	Longitude (°E)	Elevation (m)	Thick-ness cm	Shielding factor[a]	Quartz (g)	^{10}Be[b] (10^5 atoms g^{-1})	^{10}Be[c] (10^5 atoms g^{-1})	Age[d] (ka)	Loess thickness[e] (cm)	Age[f] (ka)
CN-14	Y-T6	38.81	100.17	1802	5	0.994	15.68	17.01 ± 0.29	15.86 ± 0.17	102.8 ± 6.5	45	100.6 ± 3.9

[a]*The shielding factor includes correction for horizon shielding and for the dip of the surface as well as a correction for sample thickness assuming a rock density of 2.65 g cm^{-3}.*
[b]*Measured ^{10}Be concentration of the samples.*
[c]*^{10}Be concentration has been corrected for inheritance using the estimated blank ^{10}Be concentration of 1.15 ± 0.06 × 105 atoms g^{-1}, which was derived from the modern sediments of the Heihe River by Palumbo et al. (2011).*
[d]*Exposure age calculated without correction for the loess cover (1σ) with the CRONUS-Earth ^{10}Be–^{26}Al online calculator (http://hess.ess.washington.edu/, version 2.3), using the time-dependent production rate scaling model of Lal (1991)–Stone (2000).*
[e]*Thickness of aeolian loess deposited on the gravel deposit.*
[f]*Exposure age calculated with a correction for the loess cover (1σ). This assumes a loess deposition since 12 ± 2 ka with an accumulation rate of 21.7 cm/ka (Stokes et al., 2003; Küster et al., 2006) (the uncertainty of the accumulation rate is not included); all ages were calculated assuming zero erosion.*

deposits (the strath was not identified), and the gravels are covered by > 10 m of colluvial sediments. One OSL sample (HH081603) was collected from floodplain deposits and yielded an age of 4.6 ± 0.4 ka, which is consistent with the previous dating of T2 along the mountain front (~5 ka, Li et al., 1999). Along transect YL02 (**Figure 4B**), there are three terraces (Y-T3 to Y-T5) on the valley slope, which are 17, 27, and 62 m above the present-day riverbed, respectively. Along transect YL03 (**Figure 4C**), the gravel layer of Y-T4 is 6-m-thick and covered by ~1 m of floodplain deposits. OSL sample HH081602 was collected from the floodplain deposits and yielded an age of 24.0 ± 2.1 ka, which agrees with the age of the initiation of the Y-T3 deposit (~22 ka, **Figure 4F**). On transect YL04 (**Figure 5D**), three terraces (Y-T3 to Y-T5) are 15, 25, and 68 m above the present-day riverbed, respectively. One sample from a sand interlayer on terrace Y-T5 yielded an age of ~96.0 ± 8.4 ka; however, we discarded this result because of the excessive dose rate (**Table 1**). On transect YL05 (**Figure 5E**), the highest terrace (Y-T6) was 114 m above the modern river and overlain by ~26 m of fluvial gravels, which in turn are covered by 40–50 cm of aeolian loess. One ^{10}Be exposure sample on the T6 surface (CN-14) was collected and yielded an age of 100.6 ± 3.9 ka. Y-T5 stands 97 m above the modern riverbed and the thickness of the fluvial gravels is ~20 m, which are covered by > 10 m of colluvial sediments. One sample from a sand interlayer on this terrace yielded the age of ~86.5 ± 7.8 ka; however, this result was also discarded because of the excessive dose rate (**Table 1**). Y-T4 is widespread and has a thick gravel layer (~15 m). The strath is 40 m above the modern riverbed and the terrace surface is 55 m. Terrace Y-T3 stands 44 m above the modern riverbed and the thickness of the fluvial gravels is 5 m. Along the mountain front, the NQF has dislocated the terraces of the Heihe River (**Figure 3A**). Complete staircase preservation permits the straightforward fitting between the terraces on the hanging wall and the footwall of the NQF.

Combined with the results of this study and the previous studies mentioned above, the fluvial terraces at the mountain front and the Zoulang Nan Shan sites were formed at 100.6 ± 3.9 ka (Y-T6), 24.0 ± 2.1 ka (Y-T4), 9–10 ka (Y-T3), ~5 ka (Y-T2) and 1.3 ka (Y-T1).

4.1.3 Qilian Basin Site

At the Qilian basin site, most of the terraces are incised into Cretaceous sandstone or Ordovician metamorphic rocks. The gravel layers are usually covered by floodplain deposits of sands and capped with varying depths of eolian loess. There are three lower terraces (Q-T1a, Q-T1b and Q-T1c) always co-extensive. Terrace Q-T1a is 3–5 m high above the modern river level and no suitable sample could be obtained for dating. Terrace Q-T1b is 7 m above the present-day river level and capped with 3 m of fluvial gravels (**Figure 4G**). Exposure of the Q-T1b strath is limited because of the aggradation of the T1a deposits. The strath of Q-T1c is 10 m above the river level and capped by 8 m of fluvial gravels (**Figure 4G**). Sample 2A was from fluvial sand, 30 cm above the basal gravel layer of Q-T1c and yielded an age of 12.7 ± 0.9 ka (**Figure 4G**). Utilizing OSL dating, our previous study showed that the terraces in the Qilian basin

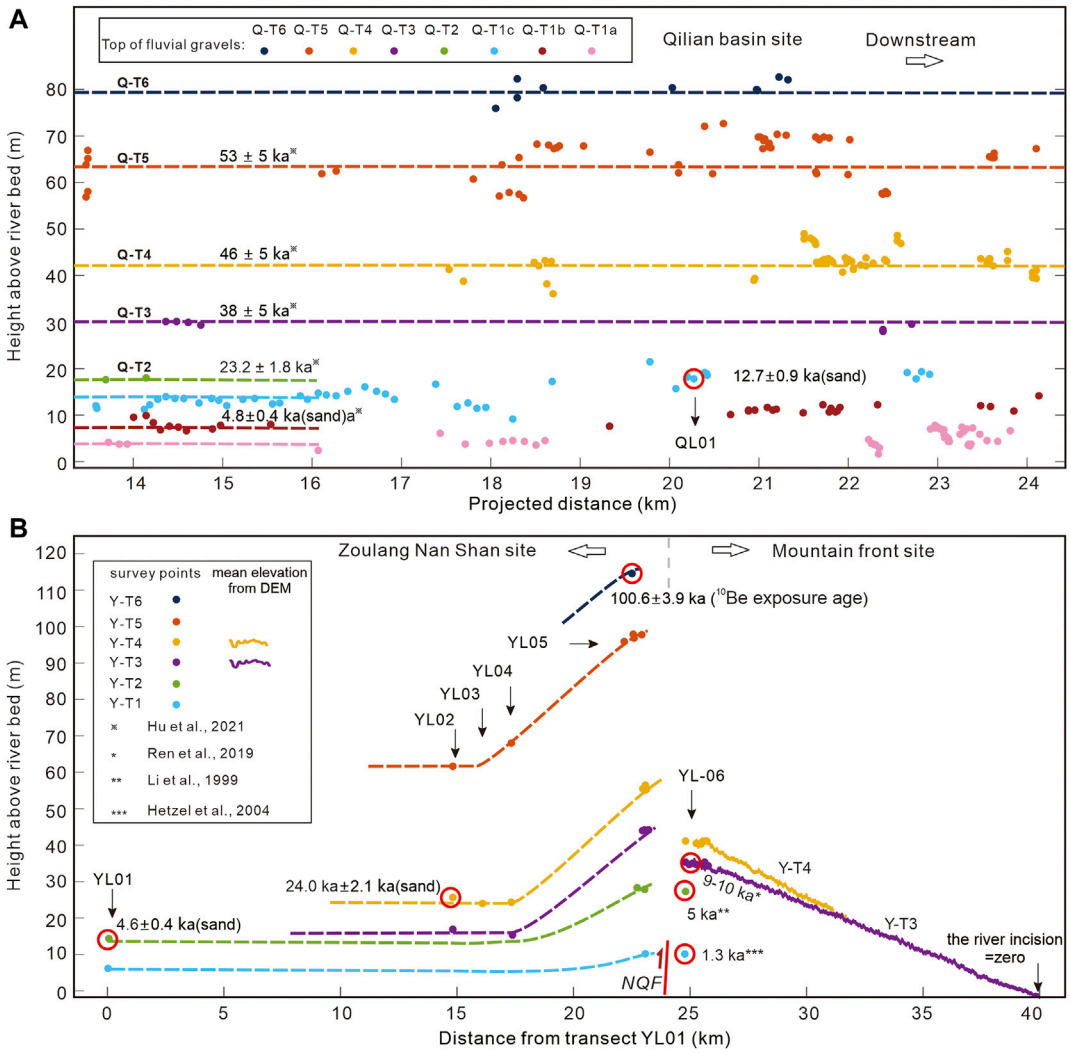

FIGURE 6 | Results of the terrace survey showing the longitudinal profiles (small colored dots) for each terrace level at the Qilian basin site **(A)**, the Zoulang Nan Shan site and the mountain front site **(B)**. The dashed lines are reconstructed pre-incision longitudinal profiles. The oscillations in the Y-T3 and T4 profiles are due to the lower resolution of the regional DEM.

TABLE 3 | River incision rates at the river mouth (transect YL05).

Terrace	Y-T1	Y-T2	Y-T3	Y-T4	Y-T5	Y-T6
Height of terrace (m)	10	28	44	55	97	114
Ages of terrace deposits or loess (ka)	1.3 ± 0.1	5[a]	9–10[b]	24.0 ± 2.1	—	100.6 ± 3.9
River incision rate (mm/yr)	7.7 ± 0.8	5.6 ± 0.7	4.6 ± 0.4	2.3 ± 0.3	—	1.1 ± 0.1

[a]*Age from Li et al. (1999).*
[b]*Ages from Li et al. (1999) and Ren et al. (2019). Incision rates (2σ) were calculated by Monte Carlo simulation (1000-times), with assuming 5% error in height of terrace.*

site were formed at 53 ± 5 ka, 46 ± 5 ka, 38 ± 5 ka, 23.2 ± 1.8 ka and 4.8 ± 0.4 ka, respectively (Hu et al., 2021). Combined with the results of this study, we conclude that the fluvial terraces in this region were formed at 53 ± 5 ka (Q-T5), 46 ± 5 ka (Q-T4), 38 ± 5 ka (Q-T3), 23 ± 2 ka (Q-T2), 12.7 ± 0.9 ka (Q-T1c) and 4.8 ± 0.4 ka (Q-T1b).

4.2 Late Quaternary Rates of River Incision

At the mouth of the Heihe River (transect YL05), the river incision rate is 1.1 ± 0.1 mm/yr for the highest terrace Y-T6 since ~100 ka (**Table 3**). For the lower terraces along transect YL05, the river incision rates since ~24, 10, 5, and 1.3 ka are 2.3 ± 0.3 mm/yr, 4.6 ± 0.4 mm/yr, 5.6 ± 0.7 mm/yr and 7.7 ± 0.8 mm/

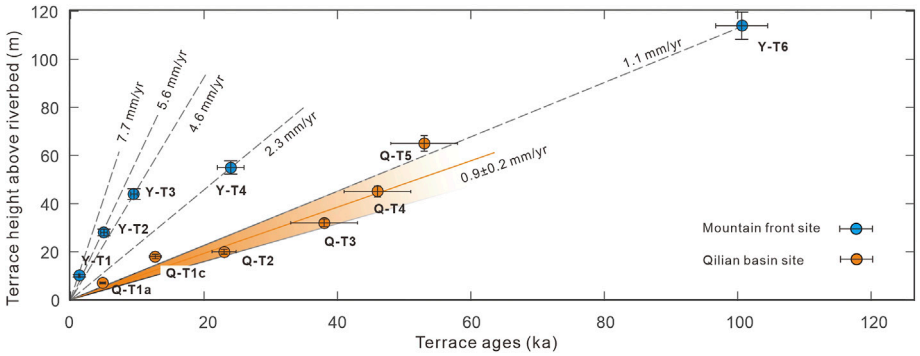

FIGURE 7 | Plot of ages versus the heights of the different terraces. The blue bars indicate the age errors. The rate of 0.9 ± 0.2 mm/yr is derived by linear fitting with 95% confidence intervals.

TABLE 4 | River incision rates at the Qilian basin site.

Terrace	Q-T1b	Q-T1c	Q-T2	Q-T3	Q-T4	Q-T5
Height of terrace (m)	7	18	20	32	45	65
Ages of terrace deposits or loess (ka)	4.8 ± 0.4[a]	12.7± 0.9	23.2 ± 1.8[a]	38 ± 5[a]	46 ± 5[a]	53 ± 5[a]
River incision rate (mm/yr)	1.5 ± 0.2	1.4 ± 0.1	0.9 ± 0.1	0.9 ± 0.1	1.0 ± 0.1	1.3 ± 0.2

[a]*Ages from Hu et al. (2021). Incision rates (2σ) were calculated by Monte Carlo simulation (1000-times), assuming a 5% error for the height of the terrace.*

yr, respectively (**Table 3**). Along transect YL03, the river incision rate is 1.0 ± 0.1 mm/yr since ~24 ka, and along transect YL01, the river incision rate is 3.5 ± 0.2 mm/yr since ~4.6 ka.

Along the Qilian basin reach, the incision rates range from 0.9 mm/yr to 1.5 mm/yr since ~53 ka, and we propose that the regional mean fluvial incision rate is 0.9 ± 0.2 mm/yr (**Figure 7**). The terrace ages define an approximately linear trend when plotted versus the heights of the terrace trend above the riverbed, suggesting that river incision has remained constant from least 53 ka to the present.

In summary, our results reveal the following spatiotemporal pattern of river incision along the Heihe River (**Figure 7**): 1) incision rates along the mountain front increased temporally from 1.1 ± 0.1 mm/yr in the late Pleistocene to 7.7 ± 0.8 mm/yr in the Holocene; 2) incision rates since ~5 ka decreased from 5.6 ± 0.7 mm/yr (YL05) to 3.5 ± 0.2 mm/yr (YL01) and 1.5 ± 0.2 mm/yr (QL01, Qilian basin), indicating that the rates of river incision during the Holocene have decreased upstream; 3) incision rates along the Qilian basin reach were constant during the late Pleistocene (0.9 ± 0.2 mm/yr). The mean heights, abandonment ages, and mean incision rates of the terraces at the mountain front and the Qilian basin are summarized in **Table 3** and **Table 4**.

5 DISCUSSION

5.1 Temporal Variations in River Incision Rates

The incision rates calculated from the fluvial terraces along the Heihe River in this study varied between 0.9 and 7.7 mm/yr since the late Pleistocene. These values are significantly higher than the landscape-scale erosion rates estimated from cosmogenic ^{10}Be concentrations in river sediments. The millennial-scale catchment-averaged denudation rates derived from the trunk are 0.3–0.4 mm/yr (Hu et al., 2015a; Palumbo et al., 2011; **Figure 1**). A possible reason for the lower ^{10}Be-derived erosion rates is the spatially weighted values over the drainage area of the Ganzhou basin (**Figure 1**). The Ganzhou basin is a piggy-back basin that was infilled with thick Quaternary deposits, suggesting that an endorheic drainage system was established here (Li, 1994). Although the Ganzhou basin is now externally drained, the upland maintains relatively low erosion rates (<0.2 mm/yr, Hetzel, 2013; Hu et al., 2015a). Another reason for the different rates estimated using the two different methods may be the lagged response of the hillslopes to a recently accelerated trunk river incision event. Along the northern margin of the Zoulang Nan Shan, the river incision rates are 5–10 mm/yr during the Holocene (Hetzel et al., 2006; Tian et al., 2017; Liu et al., 2019; Yang et al., 2020). However, denudation rates from several catchments draining the Zoulang Nan Shan are < 1 mm/yr (Palumbo et al., 2011; Hu et al., 2015a). This common phenomenon supports our view that, along the northern margin of the Zoulang Nan Shan, the landscape-scale erosion estimated from cosmogenic ^{10}Be concentrations in river sediments lags the trunk river incision rate.

A notable feature of these incision rates is that the rates calculated for the Holocene are substantially higher than those estimated over the late Pleistocene. Finnegan et al. (2014) showed that the estimated fluvial incision rates will be greater, due to the shorter measurement interval, also known as the "Sadler effect" (Sadler, 1981). However, in contrast to what would be expected

for the "Sadler effect", we observe that the incision rates in the Qilian basin are consistent during different measurement intervals. There is no reason why this effect should differentially influence the Heihe River. Consistent with an earlier compilation (Hetzel et al., 2006; Tian et al., 2017; Liu et al., 2019; Yang et al., 2020), the rates calculated over the Holocene are substantially higher than those estimated over the late Pleistocene. The longitudinal geometry of the foreland basin was interpreted to reflect climate change during the latest Pleistocene–early Holocene (Poisson and Avouac, 2004; Lu et al., 2018; Malatesta et al., 2018; Lu et al., 2020; Wang et al., 2022). During the last glacial period (17–24 ka, Osman et al., 2021), large volumes of sediment accumulated in the mountain front area, resulting in alluvial fan development (e.g., Y-T4 and Y-T3). The increasing sediment flux would be expected to cause continuous aggradation and thus the steepening of the fans. Until the warm and wet Holocene, river incision became dominant, leading to alluvial fan abandonment. The lower ratio between the sediment flux and water discharge, due to the increased precipitation, will finally result in the decrease of the river's gradient (Malatesta and Avouac, 2018; Lu et al., 2020). As a result, at the mountain front site, river incision rates for the Holocene increased significantly.

5.2 Spatial Variation of River Incision

As shown by the terrace profiles at the mountain front site, the amount of river incision is still significant and only farther north does it gradually decrease to zero (~40 km, **Figure 6B**). As a result, the spatial pattern of river incision shows a downstream-decreasing trend from the maximum where the river exits the range (**Figure 6B**).

The terrace profiles at the Zoulang Nan Shan site also show a gradual and progressive incision and increased spacing downstream (**Figure 6B**). The terrace profiles exhibit long-wavelength folds across the Qilian Shan: e.g., the western Qilian Shan (Liu et al., 2019; Wang et al., 2020) and the eastern Qilian Shan (Hu et al., 2015b; Zhong et al., 2020). Because of the fold-related increase in vertical uplift, tectonics could have maintained further river entrenchment, which may explain the increased vertical terrace spacing in the Zoulang Nan Shan. The Holocene rock uplift of the fold has been estimated to be < 10 m (with a maximum vertical uplift rate of 1 mm/yr) (Liu et al., 2019; Wang et al., 2020). Taking terrace Y-T3 (9–10 ka) as an example, the maximum vertical uplift of ~10 m is low compared to the maximum incision of ~44 m (transect YL05, **Figure 4E**). Thus, we prefer to conclude that the enhanced incision was caused not only by the differential uplift of the Zoulang Nan Shan, but also by the base level lowering of the foreland river. Furthermore, the vertical slip on the NQF and the enhanced incision would contribute the base level lowering at the mountain front. There is a clear fault scarp on terrace Y-T3, indicating that 2–3 m vertical uplift on the NQF during the Holocene (Ren et al., 2019). This vertical uplift might be ignored. Therefore, it is more likely that climate change was the main cause of the vertical spacing of the Zoulang Nan Shan terrace profiles.

According to the forgoing processes, an incisional wave resulting from climate change propagated upstream towards the range. However, along the Qilian basin reach, all terrace surfaces are approximately parallel to the modern riverbed (**Figure 6A**) and river incision has remained constant from at least ~53 ka to the present. Therefore, the incisional wave resulting from climate change only affected the river over a limited distance and has not propagated upstream towards the Qilian basin. This phenomenon further explains an earlier question in **Section 5.1**: why ^{10}Be-derived erosion from several catchments draining the Zoulang Nan Shan lags the trunk river incision. We speculate that the incision wave has not travel through much further to the upstream and affect landscape there. Thus, the equilibrium between landscape-scale erosion and river incision have not achieved yet. Unfortunately, the stream or the terrace profiles do not provide clear evidence for knickpoint migration. On the other hand, river incision in the Qilian basin is coupled with ongoing uplift driven by the fault activity of the NQF (~1 mm/yr) (Xiong et al., 2017; Cao et al., 2019). We therefore suggest that tectonic uplift driven by fault activity sets the background rate of river incision and that the climatically-induced adjustment of the longitudinal profile is limited to the downstream reach, especially along the range front.

6 CONCLUSION

We report well-preserved fluvial terraces along three reaches of the Heihe River in northeastern Tibet. At the mountain front site, river incision rate was ~1 mm/yr over the past 100 kyr, while it ranged from 2 to 7 mm/yr during the Holocene. In the interior of the mountain range (Qilian basin site), river incision rates were ~1 mm/yr since ~53 ka, suggesting that the upstream incision rate remained stable from the late Pleistocene to the Holocene. We conclude that the long-term rate of incision (since the late Pleistocene) is explained by ongoing uplift driven by fault activity, which sets the background rate of fluvial incision (~1 mm/yr). The fast incision rates during the Holocene are attributed to the progressive lowering of the river gradient induced by the warm and wet Holocene climate. The reconstructed longitudinal profiles show semi-parallel terraces in the Qilian basin, and progressively increasing terrace spacing before exiting the range, followed by decreased terrace spacing in the foreland. The most plausible explanation for this morphology is the increased fluvial discharge during the Holocene which promoted the accelerated piedmont entrenchment of the Heihe River. In turn, the enhanced incision of the Heihe River propagated upstream towards the range, but it only affected the river profile within a limited distance. Finally, the denudation rates on the millennial timescale estimated from previous studies in the region are < 1 mm/yr, suggesting that landscape-scale erosion in this region lags the trunk river incision. These results suggest that climate changes and the hydrologic response over time are important for modulating river incision rates

on various spatial and temporal scales in a tectonically active region.

DATA AVAILABILITY STATEMENT

The original contributions presented in the study are included in the article/Supplementary Material, further inquiries can be directed to the corresponding author.

AUTHOR CONTRIBUTIONS

XC wrote the first draft of the manuscript, conducted the field and lab work, and constructed the figures. XH contributed to conception and design of the study, led the field investigations. BP provided the funding and resources for this research. ZZ analyzed parts of the data. All authors contributed to manuscript revision, read, and approved the submitted version.

FUNDING

This research was financially supported by the National Natural Science Foundation of China (award 41730637, 42101004), the Strategic Priority Research Program (A) of Chinese Academy of Sciences (award XDA2010030806) and the Second Tibetan Plateau Scientific Expedition (award 2019QZKK0205).

ACKNOWLEDGMENTS

We thank Zhenling Wen, Miao Chen, Taian Chen, Xianghe Ji, Bingxue Qin, and Xiaohua Li (Lanzhou University) for their assistances with the field work. The OSL experiments were completed by Yixuan Wang (Qinghai Institute of Salt Lakes, Chinese Academy of Sciences) and Chang Huang, Yulong Ou, Min Cao (China University of Geosciences, Wuhan) and we acknowledge their careful work.

REFERENCES

Anderson, R. S., Repka, J. L., and Dick, G. S. (1996). Xplicit Treatment of Inheritance in Dating Depositional Surfaces Using *In Situ* ^{10}Be and ^{26}Al. *Geol* 24 (1), 47–51. doi:10.1130/0091-7613(1996)024<0047:etoiid>2.3.co;2

Bovet, P. M., Ritts, B. D., Gehrels, G., Abbink, A. O., Darby, B., and Hourigan, J. (2009). Evidence of Miocene Crustal Shortening in the North Qilian Shan from Cenozoic Stratigraphy of the Western Hexi Corridor, Gansu Province, China. *Am. J. Sci.* 309 (4), 290–329. doi:10.2475/00.4009.02

Burbank, D. W., and Anderson, R. S. (2011). *Tectonic Geomorphology*. second ed. Chichester: John Wiley & Sons.

Burbank, D. W., Leland, J., Fielding, E., Anderson, R. S., Brozovic, N., Reid, M. R., et al. (1996). Bedrock Incision, Rock Uplift and Threshold Hillslopes in the Northwestern Himalayas. *Nature* 379 (6565), 505–510. doi:10.1038/379505a0

Cao, X., Hu, X., Pan, B., Zhang, J., Wang, W., Mao, J., et al. (2019). A Fluvial Record of Fault-Propagation Folding along the Northern Qilian Shan Front, NE Tibetan Plateau. *Tectonophysics* 755, 35–46. doi:10.1016/j.tecto.2019.02.009

Cao, X., Hu, X., Pan, B., Zhao, Q., Chen, T. a., Ji, X., et al. (2021). Using Fluvial Terraces as Distributed Deformation Offset Markers: Implications for Deformation Kinematics of the North Qilian Shan Fault. *Geomorphology* 386, 107750. doi:10.1016/j.geomorph.2021.107750

Craddock, W. H., Kirby, E., Harkins, N. W., Zhang, H., Shi, X., and Liu, J. (2010). Rapid Fluvial Incision along the Yellow River during Headward Basin Integration. *Nat. Geosci.* 3 (3), 209–213. doi:10.1038/ngeo777

Daniels, J. M. (2008). Distinguishing Allogenic from Autogenic Causes of Bed Elevation Change in Late Quaternary Alluvial Stratigraphic Records. *Geomorphology* 101 (1-2), 159–171. doi:10.1016/j.geomorph.2008.05.022

Ferrier, K. L., Huppert, K. L., and Perron, J. T. (2013). Climatic Control of Bedrock River Incision. *Nature* 496, 206–209. doi:10.1038/nature11982

Finnegan, N. J., Schumer, R., and Finnegan, S. (2014). A Signature of Transience in Bedrock River Incision Rates over Timescales of 10(4)-10(7) Years. *Nature* 505 (7483), 391–394. doi:10.1038/nature12913

Hetzel, R., Tao, M., Stokes, S., Niedermann, S., Ivy-Ochs, S., Gao, B., et al. (2004). Late Pleistocene/Holocene Slip Rate of the Zhangye Thrust (Qilian Shan, China) and Implications for the Active Growth of the Northeastern Tibetan Plateau. *Tectonics* 23 (6), TC6006. doi:10.1029/2004tc001653

Hetzel, R., Niedermann, S., Tao, M., Kubik, P. W., and Strecker, M. R. (2006). Climatic versus Tectonic Control on River Incision at the Margin of NE Tibet: ^{10}Be Exposure Dating of River Terraces at the Mountain Front of the Qilian Shan. *J. Geophys. Res.* 111 (F3), F03012. doi:10.1029/2005jf000352

Hetzel, R. (2013). Active Faulting, Mountain Growth, and Erosion at the Margins of the Tibetan Plateau Constrained by In Situ-produced Cosmogenic Nuclides. *Tectonophysics* 582 (1), 1–24. doi:10.1016/j.tecto.2012.10.027

Hu, K., Fang, X., Zhao, Z., and Granger, D. (2015a). Erosion Rates of Northern Qilian Mountains Revealed by Cosmogenic 10 Be. *Adv. Earth Sci.* 30 (02), 268–275. doi:10.11867/j.issn.1001-8166.2015.02.0268

Hu, X., Pan, B., Kirby, E., Gao, H., Hu, Z., Cao, B., et al. (2015b). Rates and Kinematics of Active Shortening along the Eastern Qilian Shan, China, Inferred from Deformed Fluvial Terraces. *Tectonics* 34, 2478–2493. doi:10.1002/2015tc003978

Hu, X., Cao, X., Li, T., Mao, J., Zhang, J., He, X., et al. (2021). Late Quaternary Fault Slip Rate within the Qilian Orogen, Insight into the Deformation Kinematics for the NE Tibetan Plateau. *Tectonics* 40 (5), e2020TC006586. doi:10.1029/2020tc006586

Kirby, E., and Whipple, K. X. (2012). Expression of Active Tectonics in Erosional Landscapes. *J. Struct. Geol.* 44, 54–75. doi:10.1016/j.jsg.2012.07.009

Küster, Y., Hetzel, R., Krbetschek, M., and Tao, M. (2006). Holocene Loess Sedimentation along the Qilian Shan (China): Significance for Understanding the Processes and Timing of Loess Deposition. *Quat. Sci. Rev.* 25 (1), 114–125. doi:10.1016/j.quascirev.2005.03.003

Lai, Z.-P., and Wintle, A. G. (2006). Locating the Boundary between the Pleistocene and the Holocene in Chinese Loess Using Luminescence. *Holocene* 16 (6), 893–899. doi:10.1191/0959683606hol980rr

Lai, Z., Wintle, A. G., and Thomas, D. S. (2007). Rates of Dust Deposition between 50 Ka and 20 Ka Revealed by OSL Dating at Yuanbao on the Chinese Loess Plateau. *Palaeogeogr. Palaeoclimatol. Palaeoecol.* 248 (3), 431–439. doi:10.1016/j.palaeo.2006.12.013

Lal, D. (1991). Cosmic Ray Labeling of Erosion Surfaces: *In Situ* Nuclide Production Rates and Erosion Models. *Earth Planet. Sci. Lett.* 104, 424–439. doi:10.1016/0012-821x(91)90220-c

Li, Y., Li, B., and Yang, J. (1995). Late Quaternary Movement on the Heihekou Fault, West Gansu, China (In Chinese). *Acta Sci. Nat. Univ. Pekin.* 31 (03), 351–357.

Li, Y., Yang, J., Tan, L., and Duan, F. (1999). Impact of Tectonics on Alluvial Landforms in the Hexi Corridor, Northwest China. *Geomorphology* 28 (3), 299–308. doi:10.1016/s0169-555x(98)00114-7

Li, Y. L. (1994). *Mechanism and Evolution of Tectonic Landforms in the Middle Hexi Corridor (In Chinese)*. Doctor Doctor. Beijing: Beijing university.

Liu, X.-w., Yuan, D.-y., and Su, Q. (2019). Late Pleistocene Slip Rate on a Blind Thrust in the Western Qilian Shan, NW China. *Geomorphology* 345, 106841. doi:10.1016/j.geomorph.2019.106841

Lu, H., Cheng, L., Wang, Z., Zhang, T., Lü, Y., Zhao, J., et al. (2018). Latest Quaternary Rapid River Incision across an Inactive Fold in the Northern

Chinese Tian Shan Foreland. *Quat. Sci. Rev.* 179, 167–181. doi:10.1016/j.quascirev.2017.10.017

Lu, H., Wu, D., Zhang, H., Ma, Y., Zheng, X., and Li, Y. (2020). Spatial Patterns of Late Quaternary River Incision along the Northern Tian Shan Foreland. *Geomorphology* 357, 107100. doi:10.1016/j.geomorph.2020.107100

Malatesta, L. C., and Avouac, J.-P. (2018). Contrasting River Incision in North and South Tian Shan Piedmonts Due to Variable Glacial Imprint in Mountain Valleys. *Geology* 46 (7), 659–662. doi:10.1130/g40320.1

Malatesta, L. C., Avouac, J.-P., Brown, N. D., Breitenbach, S. F. M., Pan, J., Chevalier, M.-L., et al. (2018). Lag and Mixing during Sediment Transfer across the Tian Shan Piedmont Caused by Climate-Driven Aggradation-Incision Cycles. *Basin Res.* 30 (4), 613–635. doi:10.1111/bre.12267

Murray, A. S., and Wintle, A. G. (2000). Luminescence Dating of Quartz Using an Improved Single-Aliquot Regenerative-Dose Protocol. *Radiat. Meas.* 32 (1), 57–73. doi:10.1016/S1350-4487(99)00253-X

Niedermann, S., and Niedermann, S. (2002). Cosmic-Ray-Produced Noble Gases in Terrestrial Rocks: Dating Tools for Surface Processes. *Rev. Mineralogy Geochem.* 47 (1), 731–784. doi:10.2138/rmg.2002.47.16

Osman, M. B., Tierney, J. E., Zhu, J., Tardif, R., Hakim, G. J., King, J., et al. (2021). Globally Resolved Surface Temperatures since the Last Glacial Maximum. *Nature* 599 (7884), 239–244. doi:10.1038/s41586-021-03984-4

Palumbo, L., Hetzel, R., Tao, M., and Li, X. (2011). Catchment-wide Denudation Rates at the Margin of NE Tibet from In Situ-produced Cosmogenic ^{10}Be. *Terra nova.* 23 (1), 42–48. doi:10.1111/j.1365-3121.2010.00982.x

Pan, B., Burbank, D., Wang, Y., Wu, G., Li, J., and Guan, Q. (2003). A 900 k.Y. Record of Strath Terrace Formation during Glacial-Interglacial Transitions in Northwest China. *Geology* 31 (11), 957–960. doi:10.1130/g19685.1

Poisson, B., and Avouac, J. P. (2004). Holocene Hydrological Changes Inferred from Alluvial Stream Entrenchment in North Tian Shan (Northwestern China). *J. Geol.* 112 (2), 231–249. doi:10.1086/381659

Ren, J., Xu, X., Zhang, S., Ding, R., Liu, H., Liang, O., et al. (2019). Late Quaternary Slip Rates and Holocene Paleoearthquakes of the Eastern Yumu Shan Fault, Northeast Tibet: Implications for Kinematic Mechanism and Seismic Hazard. *J. Asian Earth Sci.* 176, 42–56. doi:10.1016/j.jseaes.2019.02.006

Roberts, H. M., and Duller, G. A. T. (2004). Standardised Growth Curves for Optical Dating of Sediment Using Multiple-Grain Aliquots. *Radiat. Meas.* 38 (2), 241–252. doi:10.1016/j.radmeas.2003.10.001

Sadler, P. M. (1981). Sediment Accumulation Rates and the Completeness of Stratigraphic Sections. *J. Geol.* 89 (5), 569–584. doi:10.1086/628623

Stokes, S., Hetzel, R., Bailey, R., and Mingxin, T. (2003). Combined IRSL-OSL Single Aliquot Regeneration (SAR) Equivalent Dose (D e) Estimates From Source Proximal Chinese Loess. *Quat. Sci. Rev.* 22 (10), 975–983. doi:10.1016/s0277-3791(03)00044-1

Stone, J. O. (2000). Air Pressure and Cosmogenic Isotope Production. *J. Geophys. Res.* 105 (B10), 23753–23759. doi:10.1029/2000jb900181

Tian, Q., Zheng, W., Zhang, D., Zhang, Y., Xu, B., and Huang, L. (2017). Influence of Tectonics and Climate on the Evolution of Fluvial Terraces: A Case Study of the Hongshuiba and Maying Rivers in the Northern Margin of the Qilian Mountains. *Seismol. Geol.* 39 (06), 1283–1296. doi:10.3969/j.issn.0253-4967.2017.06.013

Wang, Y., Oskin, M. E., Zhang, H., Li, Y., Hu, X., and Lei, J. (2020). Deducing Crustal-Scale Reverse-Fault Geometry and Slip Distribution from Folded River Terraces, Qilian Shan, China. *Tectonics* 39 (1), e2019TC005901. doi:10.1029/2019tc005901

Wang, Y., Oskin, M. E., Li, Y., and Zhang, H. (2022). Rapid Holocene Bedrock Canyon Incision of Beida River, North Qilian Shan, China. *Earth Surf. Dynam.* 10 (2), 191–208. doi:10.5194/esurf-10-191-2022

Xiong, J., Li, Y., Zhong, Y., Lu, H., Lei, J., Xin, W., et al. (2017). Latest Pleistocene to Holocene Thrusting Recorded by a Flight of Strath Terraces in the Eastern Qilian Shan, NE Tibetan Plateau. *Tectonics* 36 (12), 2973–2986. doi:10.1002/2017tc004648

Yang, H., Yang, X., Huang, X., Li, A., Huang, W., and Zhang, L. (2018). New Constraints on Slip Rates of the Fodongmiao-Hongyazi Fault in the Northern Qilian Shan, NE Tibet, from the 10 Be Exposure Dating of Offset Terraces. *J. Asian Earth Sci.* 151, 131–147. doi:10.1016/j.jseaes.2017.10.034

Yang, H., Yang, X., Huang, W., Li, A., Hu, Z., Huang, X., et al. (2020). ^{10}Be and OSL Dating of Pleistocene Fluvial Terraces along the Hongshuiba River: Constraints on Tectonic and Climatic Drivers for Fluvial Downcutting across the NE Tibetan Plateau Margin, China. *Geomorphology* 348, 106884. doi:10.1016/j.geomorph.2019.106884

Zheng, D., Clark, M. K., Zhang, P., Zheng, W., and Farley, K. A. (2010). Erosion, Fault Initiation and Topographic Growth of the North Qilian Shan (Northern Tibetan Plateau). *Geosphere* 6 (6), 937–941. doi:10.1130/ges00523.1

Zhong, Y., Xiong, J., Li, Y., Zheng, W., Zhang, P., Lu, H., et al. (2020). Constraining Late Quaternary Crustal Shortening in the Eastern Qilian Shan from Deformed River Terraces. *J. Geophys. Res. Solid Earth* 125 (9), e2020JB020631. doi:10.1029/2020jb020631

Conflict of Interest: The authors declare that the research was conducted in the absence of any commercial or financial relationships that could be construed as a potential conflict of interest.

Publisher's Note: All claims expressed in this article are solely those of the authors and do not necessarily represent those of their affiliated organizations, or those of the publisher, the editors and the reviewers. Any product that may be evaluated in this article, or claim that may be made by its manufacturer, is not guaranteed or endorsed by the publisher.